For Dave

# Fossil slabs attached to unsubducted fragments of the Farallon plate

Yun Wang[a,1,2], Donald W. Forsyth[a], Christina J. Rau[a], Nina Carriero[a], Brandon Schmandt[b,3], James B. Gaherty[c], and Brian Savage[d]

[a]Department of Geological Sciences, Brown University, Providence, RI 02865; [b]Department of Geological Sciences, University of Oregon, Eugene, OR 97403; [c]Lamont–Doherty Earth Observatory of Columbia University, Palisades, NY 10964; and [d]Department of Geosciences, University of Rhode Island, Kingston, RI 02881

Edited by David T. Sandwell, Scripps Institution of Oceanography, La Jolla, CA, and approved February 15, 2013 (received for review August 29, 2012)

**As the Pacific–Farallon spreading center approached North America, the Farallon plate fragmented into a number of small plates. Some of the microplate fragments ceased subducting before the spreading center reached the trench. Most tectonic models have assumed that the subducting oceanic slab detached from these microplates close to the trench, but recent seismic tomography studies have revealed a high-velocity anomaly beneath Baja California that appears to be a fossil slab still attached to the Guadalupe and Magdalena microplates. Here, using surface wave tomography, we establish the lateral extent of this fossil slab and show that it is correlated with the distribution of high-Mg andesites thought to derive from partial melting of the subducted oceanic crust. We also reinterpret the high seismic velocity anomaly beneath the southern central valley of California as another fossil slab extending to a depth of 200 km or more that is attached to the former Monterey microplate. The existence of these fossil slabs may force a reexamination of models of the tectonic evolution of western North America over the last 30 My.**

plate tectonics seismology subduction

As the Pacific–Farallon spreading center approached North America, the Farallon plate fragmented into a number of small plates (1–4). Some fragments of the Farallon plate still exist as separate plates subducting beneath North America, including the Cocos and Juan de Fuca plates, which subsequently further fragmented generating the actively subducting Rivera, Gorda, and Explorer microplates (Fig. 1). Some fragments were incorporated into the Pacific plate as subduction and spreading ceased, including the Monterey microplate and the Guadalupe and Magdalena microplate fragments of the Cocos plate (3–6). Probably subduction ceased because the sinking oceanic slab detached from the surface plate, removing the driving force of the pull from the subducting slab (7), but it has been unclear where or at what depth detachment occurred. As the plates slowed before spreading ceased entirely, the direction of relative motion between the microplates and the Pacific plate changed, causing the spreading centers (but not necessarily the microplates) to rotate. Seismic tomography imaging shows that there are high-velocity anomalies landward of the Monterey, Guadalupe, and Magdalena microplates, which we interpret as the fossil slabs still attached to the remnant oceanic microplates. The fossil Guadalupe slab extends to a depth of 130 km or more, and the Monterey slab extends deeper than 200 km.

## Results

We have generated separate tomographic images of the S velocity in the upper mantle beneath the Baja California region (8) and the southwestern United States (9) using the dispersion of teleseismic Rayleigh waves detected by arrays of seismic stations as the primary data. Because the depth of penetration of surface waves is roughly proportional to the period, by measuring the phase velocity at different periods as a function of horizontal position within the array, the 3D shear velocity can be inferred. A detailed description of the methods and data are given in *SI Text*.

The shear wave velocity at a depth of 100 km beneath Baja California is shown in Fig. 2. The high-velocity anomaly reaches maximum contrast at this depth, about 5% faster than the average background velocity. No high-velocity anomaly is detected at 60 km, or resolved at depths greater than 160 km. Our best estimate is that the anomalies extend to a depth of about 150 km, but the maximum depth could be as shallow as ~130 km or it could extend significantly deeper than 150 km and just escape detection. Note that there is no high-velocity anomaly beneath northern Baja California where the spreading center intersected the trench and a slab gap formed. The anomaly does not extend the entire length of the Magdalena microplate, terminating before the southern end.

In the case of the southwestern United States, there is a higher density of seismic stations (70 km or less spacing) that provide better resolution of the structure from surface waves as well as good body wave tomography, so in that area, we improved the deeper part of the imaging by iterating back and forth between surface wave and body wave imaging. There are three pronounced high-velo[redacted]*A*): the root to the core of the Colorado plateau; the Transverse Range anomaly; and the anomaly centered at 36.5°N, 119.5°W, which has variously been described as the Isabella anomaly, the southern Central Valley anomaly, the southern Great Valley anomaly, or the South Sierra Nevada anomaly (10–16). In addition, there is a very low-velocity anomaly (<3.9 km/s) along coastal California at about 39°N. This and other low-velocity regions inland at this depth are associated with Quaternary volcanism. At 100 km, the Transverse Range anomaly is much weaker, with the Isabella anomaly and the Colorado plateau root remaining as strong, high-velocity anomalies (Fig. 3*B*). The Transverse Range anomaly has been interpreted as being caused by convergence between the Pacific and North American plates forcing the lithosphere downward in the vicinity of the bend in the San Andreas fault (17). Our focus is primarily on the Isabella anomaly.

## Discussion

The Isabella anomaly has usually been interpreted as either a continental lithospheric convective drip or as delaminating lithosphere from beneath the Sierra Nevada (10, 12, 13, 18), although there was an early suggestion that a slab fragment from Laramide or post-Laramide time could contribute to the anomaly (11). A cross-section through the Isabella anomaly (Fig. 3*C*)

Author contributions: D.W.F. and J.B.G. designed research; Y.W., D.W.F., C.J.R., B. Schmandt, J.B.G., and B. Savage performed research; Y.W., D.W.F., C.J.R., N.C., and B. Schmandt analyzed data; and Y.W. and D.W.F. wrote the paper.

The authors declare no conflict of interest.

This article is a PNAS Direct Submission.

[1]Present address: Geophysical Institute, University of Alaska, Fairbanks, AK 99775.

[2]To whom correspondence should be addressed. E-mail: nubeyun@gmail.com.

[3]Present address: Department of Earth and Planetary Sciences, University of New Mexico, Albuquerque, NM 87131.

This article contains supporting information online at www.pnas.org/lookup/suppl/doi:10.1073/pnas.1214880110/-/DCSupplemental.

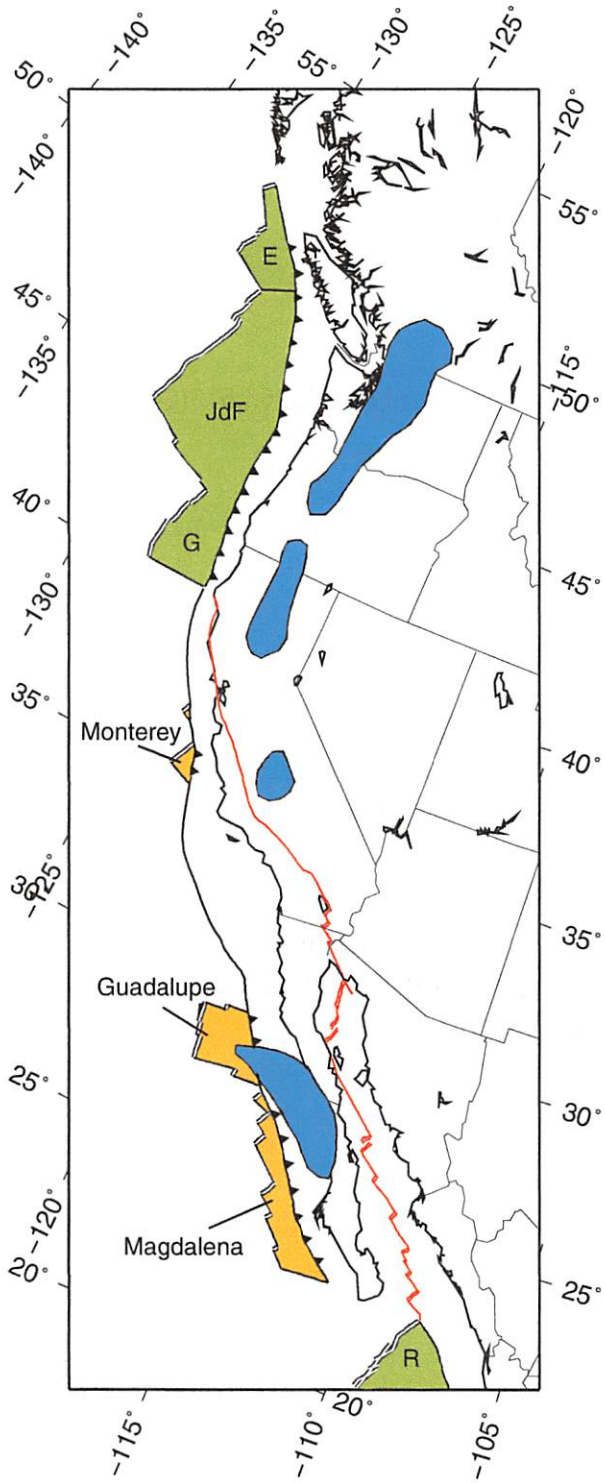


**Fig. 1.** Fragments of the Farallon plate and high seismic velocity anomalies at 100 km (blue). Velocity anomaly outlines for the northern three blue areas are based on P-wave tomography (19). Southernmost outline is from this study. Active microplates (green) still subducting are Explorer (E), Juan de Fuca (JdF), Gorda (G), and Rivera (R). Fossil microplates now incorporated into the Pacific plate are shaded orange. Current North America–Pacific plate boundary is shown in red. Spreading centers, double lines; transform faults, single lines; subduction zones, lines with triangles pointing in the direction of subduction.

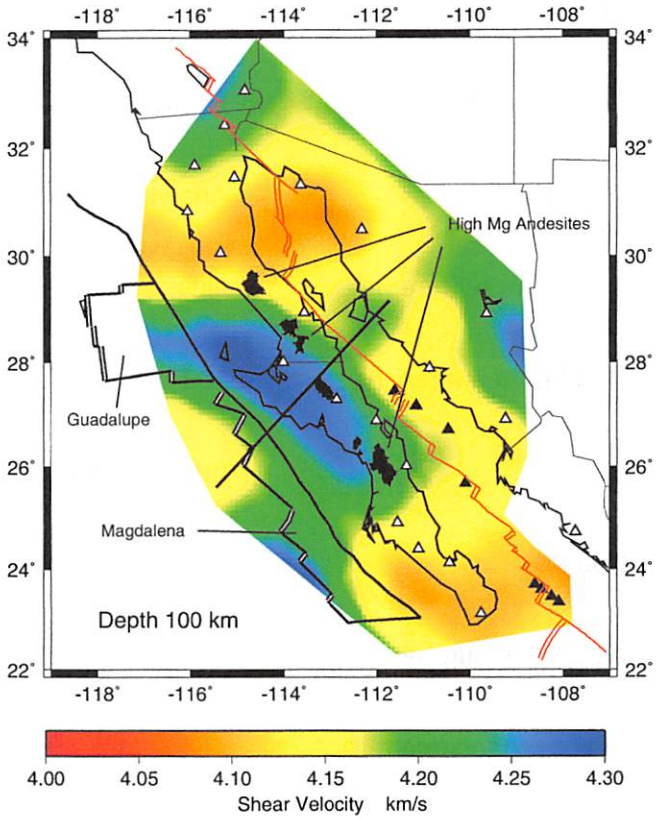


**Fig. 2.** Shear velocity anomalies at depth of 100 km and the distribution of postsubduction high-Mg andesites (black) in Baja California (23). Schematic cross-section along the straight line is shown in Fig. 4*A*. Outlines of the Guadalupe and Magdalena microplates are adapted from refs. 6 and 35. Open, upright triangles are land stations, and closed symbols are ocean-bottom seismographs.

shows that it is most pronounced at depths of less than 125 km beneath the Central Valley and western Sierra Nevada. At 100 km, the lateral velocity contrast in shear velocity with the low-velocity asthenosphere is on the order of 6%, similar to that beneath Baja California. With somewhat smaller velocity contrast, below 125 km it dips steeply downward to the east to depths greater than 200 km beneath the eastern Sierra Nevada and Owens Valley, consistent with previous body and surface wave imaging (13–16). In this paper, we interpret it as representing a fossil slab connected to the Monterey microplate.

Our interpretation of the high-velocity Isabella and central Baja California anomalies as fossil slabs attached to unsubducted microplates is illustrated in Fig. 4, which also shows a schematic cross-section through the slab gap at 39°N, just south of the Mendocino triple junction between the Pacific, North American, and Juan de Fuca or Gorda plates. One of the strongest pieces of evidence for this interpretation is simply the geometry of the anomalies and the remnant microplates (Fig. 1). At 100-km depth, the high-velocity anomalies along the west coast of North America are all either associated with the actively subducting Juan de Fuca/Gorda plate or directly opposite unsubducted microplates. The distance from the fossil trenches to the anomalies is similar to the distance from the active trench to the subducting Juan de Fuca slab and the velocity contrasts with surrounding asthenosphere are nearly the same (19).

Previous interpretations of the Isabella anomaly as delaminated lithosphere were based largely on the proximity of the anomaly to the southern Sierra Nevada where the lower crust and lithospheric mantle on the east side of the Sierra appear to

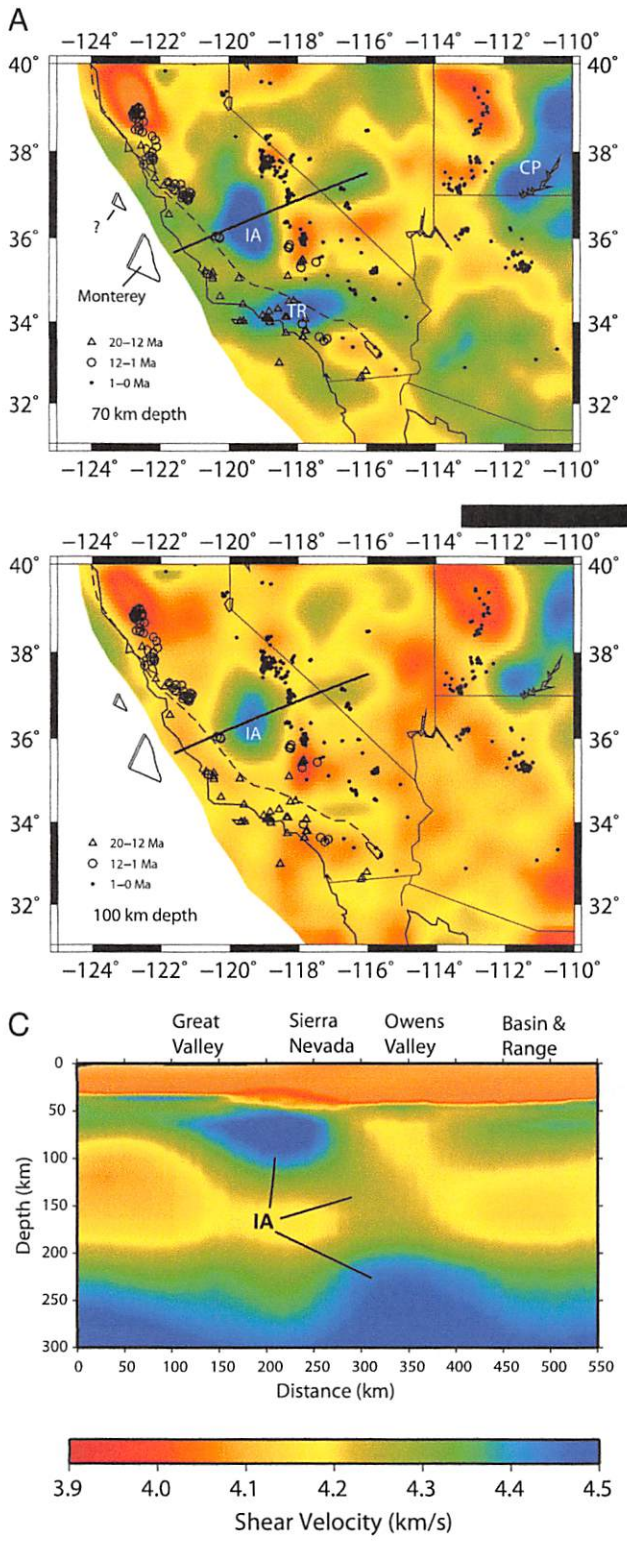


**Fig. 3.** Shear velocity anomalies in the southwestern United States. (*A*) Shear velocity at 70 km. IA, Isabella Anomaly; CP, Colorado Plateau; TR, Transverse Range. The small symbols indicate volcanic activity in different age ranges, but only the youngest activity is shown except near the coast. The dashed line is San Andreas fault. The heavy line is location of cross-section in *C*. (*B*) Shear velocity at 100-km depth. (*C*) Velocities in cross-section along line shown in *A*. The copper colors are low-velocity continental crust. The red zone above Isabella anomaly is thought to be eclogitic lower crust. Shown with a question mark is a possible second fragment of the Monterey microplate (5, 35).

have been removed, on the coinciding subsidence of the Central Valley, and on the existence of a "hole" in the P-to-S wave conversion at the Moho above part of the Isabella anomaly. The absence of a Ps signal could be caused by a steeply dipping Moho pulled down by a dripping lower lithosphere (18). However, later work showed that this weak Ps conversion is not confined to the vicinity of the Isabella anomaly; it extends along the entire western Sierra Nevada and is now thought to be due to the presence of a dense mafic–ultramafic residue in the lower crust that reduces the contrast between crust and mantle (20), an interpretation that is consistent with our tomography model that has unusually high S-wave velocities in the lower crust beneath the western Sierra Nevada (Fig. 3*C*). The subsidence in the Central Valley could be a flexural effect caused by uplift of the adjacent southern Sierra Nevada or it could be driven by slight negative buoyancy of the underlying fossil slab. To explain why the anomaly is beneath the Central Valley instead of directly beneath the eastern Sierra or left behind farther to the east beneath the Basin and Range as the continent moved westward, Zandt (12) invoked an ad hoc "mantle wind" that displaced the anomaly to the west. Our interpretation [redacted] consistent with the model of Nicholson et al. (5) in which drag from the still attached Monterey slab moving with the Pacific plate was responsible for the rotation of the overlying Transverse Ranges crustal block.

The high-velocity anomalies are expected to be due to a combination of oceanic lithosphere dehydration and cooler temperatures. The asthenosphere or low-velocity zone beneath most of southwestern North America has very low shear wave wave velocities similar to those beneath the East Pacific Rise and high Vp/Vs ratios, suggesting the presence of a small melt fraction (8, 9, 14). The oceanic lithosphere, however, is depleted and dehydrated in the process of formation of the oceanic crust, leading to higher electrical resistivity and higher seismic velocities beneath young seafloor than expected from conductive cooling alone (21). Even though the young Monterey plate stopped subducting at ~19–20 Ma (2, 4) and would now only have an average temperature contrast with the surrounding asthenosphere of 100–250 °C (22), there should be a velocity contrast with the asthenosphere throughout the 60- to 70-km thickness of depleted, subducted lithosphere caused by the absence of melting and dissolved water.

Postsubduction volcanism in Baja California is also consistent with the high-velocity anomalies being fossil slabs. The distribution of high-magnesium (Mg) andesites (bajaites), which are commonly thought to form from a mixture of magmas from melting subducted oceanic crust and melting the asthenospheric mantle wedge fluxed by hydrous fluids released from the subducted plate (23), coincides with the landward edge of the slab high-velocity anomaly at 100 km (Fig. 2). Although there is debate about their origin (24, 25), the bajaites are produced where the top edge of the slab with the basaltic crust lies directly below at a depth typical for the formation of arc volcanism. Most of the high-Mg andesites were produced millions of years after subduction ceased. The heat necessary to melt basaltic crust may have been supplied by upwelling associated with opening the Gulf of California or by replacing the detached lithosphere with hot asthenosphere at the end of the broken, fossil slab. A seismic refraction profile at 24°S suggests that detachment of the slab in that area occurred much shallower, at a depth of about 20 km (26), in agreement with the absence of high velocities and the lack of bajaites at that latitude (Fig. 2).

A different pattern of volcanism is expected for the Monterey microplate. The Guadalupe/Magdalena fossil slab is on the Pacific side of the current Pacific–North America plate boundary, but the Monterey slab is on the North American side of the San Andreas fault, marking the Pacific–North America boundary in California (Fig. 1). There is no reported postsubduction volcanism between the San Andreas fault and the coast along the corridor where

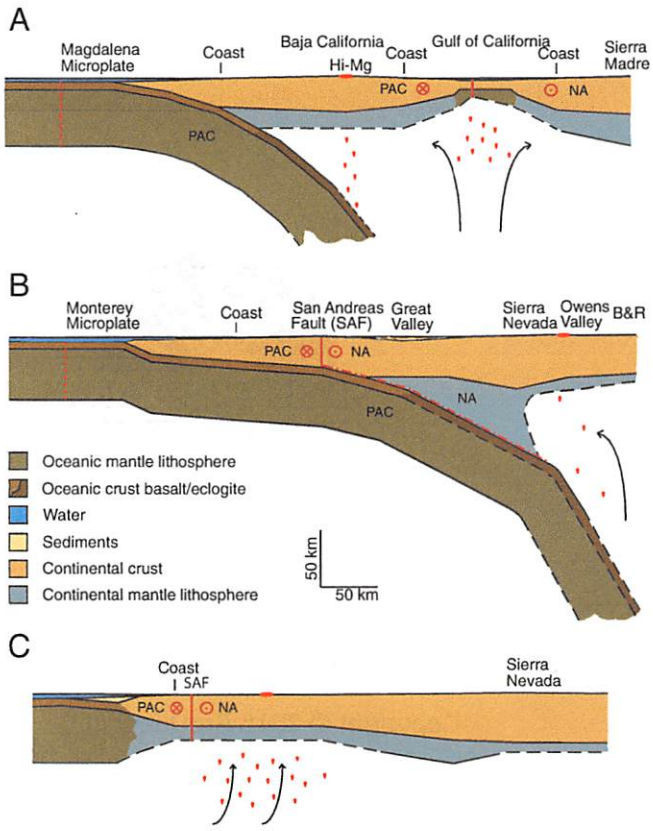


**Fig. 4.** Schematic diagrams of Magdalena fossil slab (*A*), Monterey fossil slab (*B*), and slab window south of the Juan de Fuca plate at 39°N (*C*). Location of profiles *A* and *B* are shown in Figs. 2 and 3*A*, separately. The solid red vertical line shows current Pacific–North America plate boundary. The dashed vertical red lines show location of fossil spreading centers. The arrows indicate likely mantle upwelling. The small red blobs show regions of melt production and migration. The red symbols at top indicate locations of volcanic activity at the surface not on plate boundaries.

the connection between the microplate and Isabella should lie (Fig. 3*A*). The mantle shear wave velocities are also relatively high down to depths of ~70 km in this corridor, unlike the velocities to the north of the Monterey microplate, suggesting an intact plate. Throughout this corridor, oceanic crust has been traced from the fossil trench to near the San Andreas fault using seismic refraction techniques (27), further supporting the conclusion that there is oceanic lithosphere connecting the microplate and the Isabella anomaly. The existence of this volcanic gap suggests the lithospheric blocks between the San Andreas and the coast largely translated along with the Monterey microplate and the rest of the Pacific plate, with relatively little offset on the intervening strike-slip faults.

Detachment of the slab at depth rather than near the surface may occur because young, depleted oceanic lithosphere is buoyant (28, 29). As the spreading center approaches the trench, the young upper parts of the slab thus may resist sinking while the deeper, older, colder, denser parts may pull away. Recent dynamic models of shallow detachment have not considered the effects of compositional buoyancy (7). A major remaining question is whether fossil slabs could remain attached to the microplates while translating hundreds of kilometers laterally beneath the North American plate since subduction ceased. A simple geodynamic model indicates that a cool, dehydrated plate should be sufficiently viscous that it would remain nearly undeformed (30). The temperature contrast with the surrounding asthenosphere (22) and dehydration increase the viscosity, and the effective viscosity contrast is further enhanced by the reduction in strain rate within the no-longer subducting slab if the dominant deformation mechanism is dislocation creep. Detached slabs are expected to have at least two orders of viscosity contrast with the surrounding asthenosphere (31). Depletion buoyancy and the increase in viscosity due to dehydration may be responsible for the survival of other fossil slabs, such as the 55-Ma Siletzia slab in the Pacific Northwest (32).

In summary, we have shown that there are high-velocity anomalies extending as deep as 200 km into the mantle associated with unsubducted microplates that are most simply interpreted as fossil slabs and that the fossil slabs probably influence the subsequent, postsubduction, magmatic activity.

## Materials and Methods

We use the two-plane-wave method for regional surface wave tomography (33, 34). Details of the data, procedures, and model resolution pertaining to each study area are presented in the supplementary materials to refs. 8 and 9. Briefly, we use Born approximation sensitivity kernels to predict the perturbations of the wavefield caused by heterogeneities within the region of interest, and then invert the amplitude and phase of the Rayleigh waves on an array of stations for the phase velocity and azimuthal anisotropy as a function of position as well as wave parameters describing the structure of the incoming wave field from each earthquake source. The study regions are divided into slightly overlapping subregions with independent wave parameters so that the total wavefield is allowed to be more complex. The 2D maps of phase velocity as a function of frequency are then inverted point by point to generate 3D models of vertically polarized S wave velocity.

In the case of the Baja California region, we have supplemented the original data set that used 6 y of records of teleseismic earthquakes using land stations (8) with 1 y of recordings from ocean bottom seismographs (OBS) in the central and southern Gulf of California. The combined distribution of source events and stations is shown in Figs. S1 and S2. Seventy-eight events were recorded by land stations only, and 36 events from October 2005 to October 2006 were recorded by both the Network of Autonomously Recording Seismographs (NARS)–Baja array as well as eight OBS that were part of the Sea of Cortez Ocean Bottom Array (SCOOBA) experiment. Adding the OBS records gives better resolution of velocity within the Gulf and of the southern extent of the high-velocity anomaly associated with the Guadalupe and Magdalena microplates. In the Baja region, station spacing varied from about 70 to 250 km and some of the stations were of poor quality or had more limited frequency response, yielding poorer horizontal and vertical resolution than in the southwestern United States. Phase velocities were estimated at periods ranging from 22 to 111 s.

The maximum depth extent of the fossil slab beneath Baja California is poorly known, because with the limited period range available here and the lack of body wave information, the nominal resolving length at a depth of 150 km is on the order of 100 km, i.e., the average velocity is resolvable only from ~110 to 210 km when 150 km is the target depth. In our study, resolution tests indicate that narrow, linear features would be spread out over a width of about 80 km, or about the width of the highest velocity anomalies we image, so the actual minimum width of the feature cannot be resolved. Also, any abrupt lateral termination of structure is spread out due to the limited horizontal resolution, but it is clear that the southern end of the high-velocity anomaly does not extend as far south as the southern end of the Magdalena microplate.

In the case of the southwestern United States (9), there is a higher density of seismic stations (70 km or less spacing) that provide better resolution of the structure from surface waves as well as for good body wave tomography, so in that area, we improved the deeper part of the imaging by iterating back and forth between surface wave and body wave imaging. For the surface wave analysis, we used 113 source events recorded at as many as 174 stations for an individual event, but more than 200 stations in total. Somewhere between 100 and 150 km is the crossover depth between fundamental mode surface wave and body wave resolution. At shallower depths, surface waves have much better depth resolution (using periods 18–145 s in the southwest), whereas at greater depths, body wave resolution is better, particularly of lateral variations in structure, although both have some sensitivity to velocity structure throughout the crust and upper mantle. Teleseismic body wave tomography is primarily sensitive to lateral changes in velocity, whereas surface waves provide some control on the absolute velocities. We began with a 3D SV image of Rau and Forsyth (9), and then used that model as a starting model for an S velocity model using the body wave data of Schmandt and Humphreys (15). That model was then used as a starting model for another Rayleigh wave inversion. We iterated three times, ending with a final image that is fully compatible with the Rayleigh wave data.

**ACKNOWLEDGMENTS.** This research was supported by National Science Foundation Grants OCE 0947870, EAR 0745972, and EAR 04-36411. Seismic data were supplied by Earthscope's Transportable Array in the United States and the NARS–Baja and Red Sismológica de Banda Ancha (RESBAN) arrays in Mexico. Data on volcanism were supplied by the North American Volcanic and Intrusive Rock Database (NAVDAT).

1. Atwater T (1970) Implications of plate tectonics for the Cenozoic tectonic evolution of western North America. *Bull Geol Soc Amer* 81:3513–3536.
2. Atwater T, Stock JM (1998) Pacific-North America plate tectonics of the Neogene southwestern United States. *Int Geol Rev* 40:375–402.
3. Lonsdale P (1989) *The Eastern Pacific Ocean and Hawaii*, eds Hussong D, Winterer EL, Decker RW (Geological Society of America, Boulder, CO), pp 499–522.
4. Lonsdale P (1991) *The Gulf and Peninsular Province of the Californias*, eds Dauphin JP, Simoneit BRT (AAPG, Tulsa, OK), pp 87–125.
5. Nicholson C, Sorlien CC, Atwater T, Crowell JC, Luyendyk BP (1994) Microplate capture, rotation of the western Transverse Ranges, and initiation of the San Andreas transform as a low-angle fault system. *Geology* 22:491–495.
6. Michaud F, et al. (2006) Oceanic-ridge subduction vs. slab break off: Plate tectonic evolution along the Baja California Sur continental margin since 15 Ma. *Geology* 34: 13–16.
7. Burkett ER, Billen MI (2009) Dynamics and implications of slab detachment due to ridge-trench collision. *J Geophys Res* 114:B12402.
8. Wang Y, Forsyth DW, Savage B (2009) Convective upwelling in the mantle beneath the Gulf of California. *Nature* 462(7272):499–501.
9. Rau CJ, Forsyth DW (2011) Melt in the mantle beneath the amagmatic zone, southern Nevada. *Geology* 39:975–978.
10. Aki K (1982) Three-dimensional seismic inhomogeneities in the lithosphere and asthenosphere: Evidence for decoupling in the lithosphere and flow in the asthenosphere. *Rev Geophys* 20:161–170.
11. Biasi GP, Humphreys ED (1992) P-wave image of the upper mantle structure of central California and southern Nevada. *Geophys Res Lett* 19:1161–1164.
12. Zandt G (2003) The southern Sierra Nevada drip and the mantle wind direction beneath the southwestern United States. *Int Geol Rev* 45:213–224.
13. Boyd OS, Jones CH, Sheehan AF (2004) Foundering lithosphere imaged beneath the southern Sierra Nevada, California, USA. *Science* 305(5684):660–662.
14. Yang Y, Forsyth DW (2006) Rayleigh wave phase velocities, small-scale convection, and azimuthal anisotropy beneath southern California. *J Geophys Res* 111:B07306.
15. Schmandt B, Humphreys ED (2010) Seismic heterogeneity and small-scale convection in the southern California upper mantle. *Geochem Geophys Geosyst* 11:Q05004.
16. Obrebski M, Allen RM, Pollitz F, Huang S-H (2011) Lithosphere-asthenosphere interaction beneath the western United States from the joint inversion of body-wave traveltimes and surface-wave phase velocities. *Geophys J Int* 185:1003–1021.
17. Bird P, Rosenstock RW (1984) Kinematics of present crust and mantle flow in southern California. *Geol Soc Am Bull* 95:946–957.
18. Zandt G, et al. (2004) Active foundering of a continental arc root beneath the southern Sierra Nevada in California. *Nature* 431(7004):41–46.
19. Burdick S, et al. (2010) Model update December 2009: Upper mantle heterogeneity beneath North America from P-wave travel time tomography with global and USArray Transportable Array data. *Seismol Res Lett* 81:638–645.
20. Frassetto AM, et al. (2011) Structure of the Sierra Nevada from receiver functions and implications for lithospheric foundering. *Geosphere* 7(4):898–921, 10.1130/GES00570.1.
21. Evans RL, et al. (2005) Geophysical evidence from the MELT area for compositional controls on oceanic plates. *Nature* 437(7056):249–252.
22. van Wijk JW, Govers R, Furlong KP (2001) Three-dimensional thermal modeling of the California upper mantle: A slab window vs. stalled slab. *Earth Planet Sci Lett* 186: 175–186.
23. Negrete-Aranda R, Cañón-Tapia E (2008) Post-subduction volcanism in the Baja California Peninsula, Mexico: The effects of tectonic reconfiguration in volcanic systems. *Lithos* 102:392–414.
24. Pallares C, et al. (2008) Temporal geochemical evolution of Neogene volcanism in northern Baja California (27°-30°N): Insights on the origin of post-subduction magnesian andesites. *Lithos* 105:162–180.
25. Castillo PR (2008) Origin of the adakite-high NB basalt association and its implications for post-subduction magmatism in Baja California, Mexico. *Geol Soc Am Bull* 120: 451–462.
26. Brothers D, et al. (2012) Farallon slab detachment and deformation of the Magdalena Shelf, southern Baja California. *Geophys Res Lett* 39:L09307, 10.1029/2011GL050828.
27. Brocher TM, ten Brink US, Abramovitz T (1999) Synthesis of crustal seismic structure and implications for the concept of a slab gap beneath coastal California. *Int Geol Rev* 41:263–274.
28. Cloos M (1993) Lithospheric buoyancy and collisional orogenesis: Subduction of oceanic plateaus, continental margins, island arcs, spreading ridges, and seamounts. *Geol Soc Am Bull* 105:715–737.
29. Afonso JC, Ranalli G, Fernandez M (2007) Density structure and buoyancy of the oceanic lithosphere revisited. *Geophys Res Lett* 34:L10302, 10.1029/2007GL029515.
30. Pikser JE, Forsyth DW, Hirth G (2011) Along-strike translation of a fossil slab. *Earth Planet Sci Lett* 331:315–321.
31. Liu L, Stegman DR (2011) Segmentation of the Farallon slab. *Earth Planet Sci Lett* 311: 1–10.
32. Schmandt B, Humphreys E (2011) Seismically imaged relict slab from the 55 Ma Siletzia accretion to northwest United States. *Geology* 39:175–178.
33. Forsyth DW, Li A (2005) *Geophysical Monograph Series*, eds Levander A, Nolet G (AGU, Washington, DC), Vol 157, pp 81–98.
34. Yang Y, Forsyth DW (2006) Regional tomographic inversion of amplitude and phase of Rayleigh waves with 2-D sensitivity kernels. *Geophys J Int* 166:1148–1160.
35. Tian L, et al. (2011) Petrology and Sr-Nd-Pb-He isotope geochemistry of postspreading lavas on fossil spreading axes off Baja California Sur, Mexico. *Geochem Geophys Geosyst* 12:Q0AC10.